

Shear-Wave Attenuation Study in the South Region of the Gulf of California, Mexico

by Raúl R. Castro, Shri K. Singh, Anand Joshi, and Sandeep Singh

Abstract We study the variability of the quality factor Q_S with depth (1D model) using S -wave recordings from regional stations of the Broadband Seismological Network of the Gulf of California (GoC) (RESBAN) operated by Centro de Investigación Científica y de Educación Superior de Ensenada (CICESE). We analyzed earthquakes located by [Sumy et al. \(2013\)](#) in the southern gulf with hypocenters determined using ocean-bottom seismographs of the Sea of Cortez Ocean Bottom Array (SCOoba) experiment and onshore stations of the Network of Autonomously Recording Seismographs (NARS)-Baja array. We also used events relocated by [Castro et al. \(2017b\)](#) in the same region. This catalog of seismicity within the North America–Pacific plate boundary permits us to study the attenuation characteristics of the S waves in greater detail than previous studies, because the new data set samples more densely the gulf region. We determined nonparametric attenuation functions in the 10–250 km distance range to estimate Q_S at different frequencies and depths. To estimate Q_S , the geometrical spreading function $G(r)$ is taken as $1/r$ for $r < 100$ km and $1/\sqrt{r}$ for $r \geq 100$ km. We found that at 4 Hz $Q_S \sim 770$ for the first 5 km, increasing to ~ 1200 up to 10 km depth, where Q_S starts to gradually decrease, reaching a value of $Q_S \sim 970$ between 25 and 40 km depth. This increase in attenuation at 10–40 km depth is consistent with estimates of Q_S near the East Pacific Rise ([Yang et al., 2007](#)). In general, our average estimates of Q_S , which include spreading centers and basins, are higher than those reported in other ridge zones. This indicates that zones of high attenuation in the GoC may be restricted to regions near the spreading centers. We also used the function $G(r) = 1/r$, which corresponds to the dominance of body waves at all distances, and we found that at low frequencies ($f < 4$ Hz) this function gives similar values of Q_S as those estimated with the spreading function that introduces a weaker decay with distance at $r > 100$ km.

Introduction

The Gulf of California (GoC) is located in the northwest region of Mexico (Fig. 1) along the plate boundary between the Pacific and North American plates, south of the San Andreas fault system and north of the East Pacific Rise. The gulf is an extensional province where marine basins were formed as a result of the extension and continental separation ([Stock and Hedges, 1989](#); [Osokin et al., 2001](#)). Thus, the crustal structure at the margins is different than within the gulf ([Lizarralde et al., 2007](#)). The southern region of the gulf is characterized by being very seismically active and composed by ridge centers connected by transform faults ([Thatcher and Brune, 1971](#); [Lonsdale, 1989](#); [Axen and Fletcher, 1998](#)).

We study in this article the 1D variability of the quality factor Q_S with depth of S waves using regional stations of the Broadband Seismological Network of the GoC (RESBAN) operated by Centro de Investigación Científica y de

Educación Superior de Ensenada (CICESE). We analyzed earthquakes located by [Sumy et al. \(2013\)](#) in the southern gulf with hypocenters determined by combining seismograms from an array of ocean-bottom seismographs (OBSSs), of the Sea of Cortez Ocean Bottom Array (SCOoba) experiment, with onshore stations of the Network of Autonomously Recording Seismographs (NARS)-Baja array. We also used additional earthquakes relocated by [Castro et al. \(2017b\)](#) in the same region.

The estimate of the attenuation structure is in general important because it permits us to identify low- Q_S zones that may be related with the presence of fluids or with tectonic processes relevant for understanding the crustal structure. Regional Q_S models are also useful for engineering ground-motion prediction models at regional distances. For instance, [Eberhart-Phillips et al. \(2010\)](#) noticed that the variability in

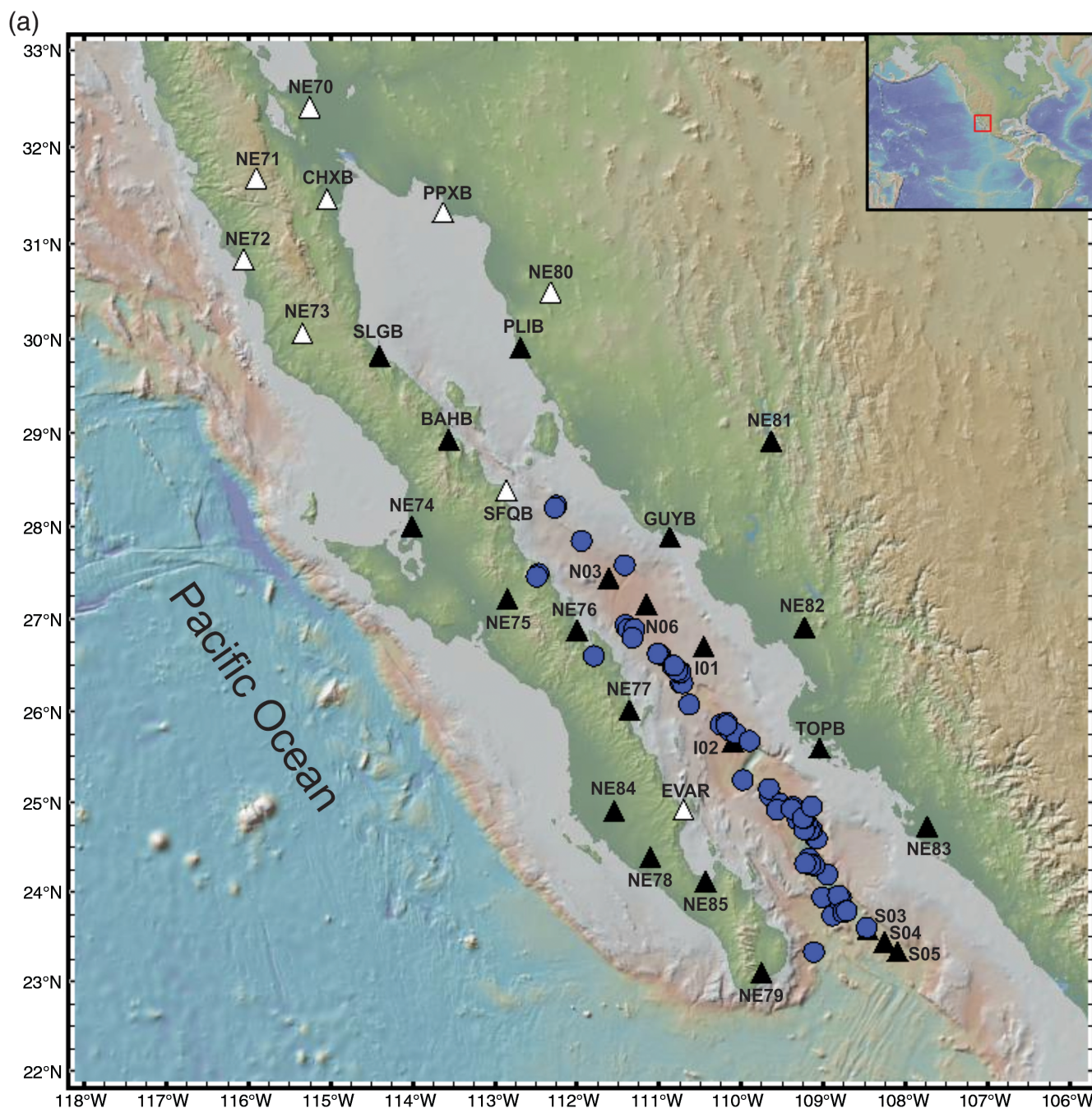


Figure 1. (a) The distribution of stations used on land (black triangles) of the Broadband Seismological Network of the Gulf of California (RESBAN) seismic network operated by Centro de Investigación Científica y de Educación Superior de Ensenada (CICESE). The inset (upper right) shows the global location of the Gulf of California (GoC) region. White triangles are stations not used in this study. The stations within the gulf are from an array of ocean-bottom seismographs of the Sea of Cortez Ocean Bottom Array (SCOoba) experiment. Circles are the epicenters used in this study, which are located in the central-south region of the Gulf of California, Mexico. (b) The location of the main ridges and transform faults of the region. The bathymetry and topography are from GeoMap App. The color version of this figure is available only in the electronic edition. *(Continued)*

the estimated attenuation rates from observations at regional distance (> 200 km) in the New Zealand's South Island can be attributed to the attenuation rate variability of the 3D Q model of Eberhart-Phillips *et al.* (2008).

Estimates of Q_S are also useful for strong ground motion studies. Recent ground-motion prediction equations include

specific anelastic attenuation terms as a function of Q_S that permit us to account for regional differences in attenuation (e.g., Graizer and Kalkan, 2015).

The attenuation of S waves in the south-central region of the GoC has been studied before by Vidales-Basurto *et al.* (2014), using the same stations but with a smaller data

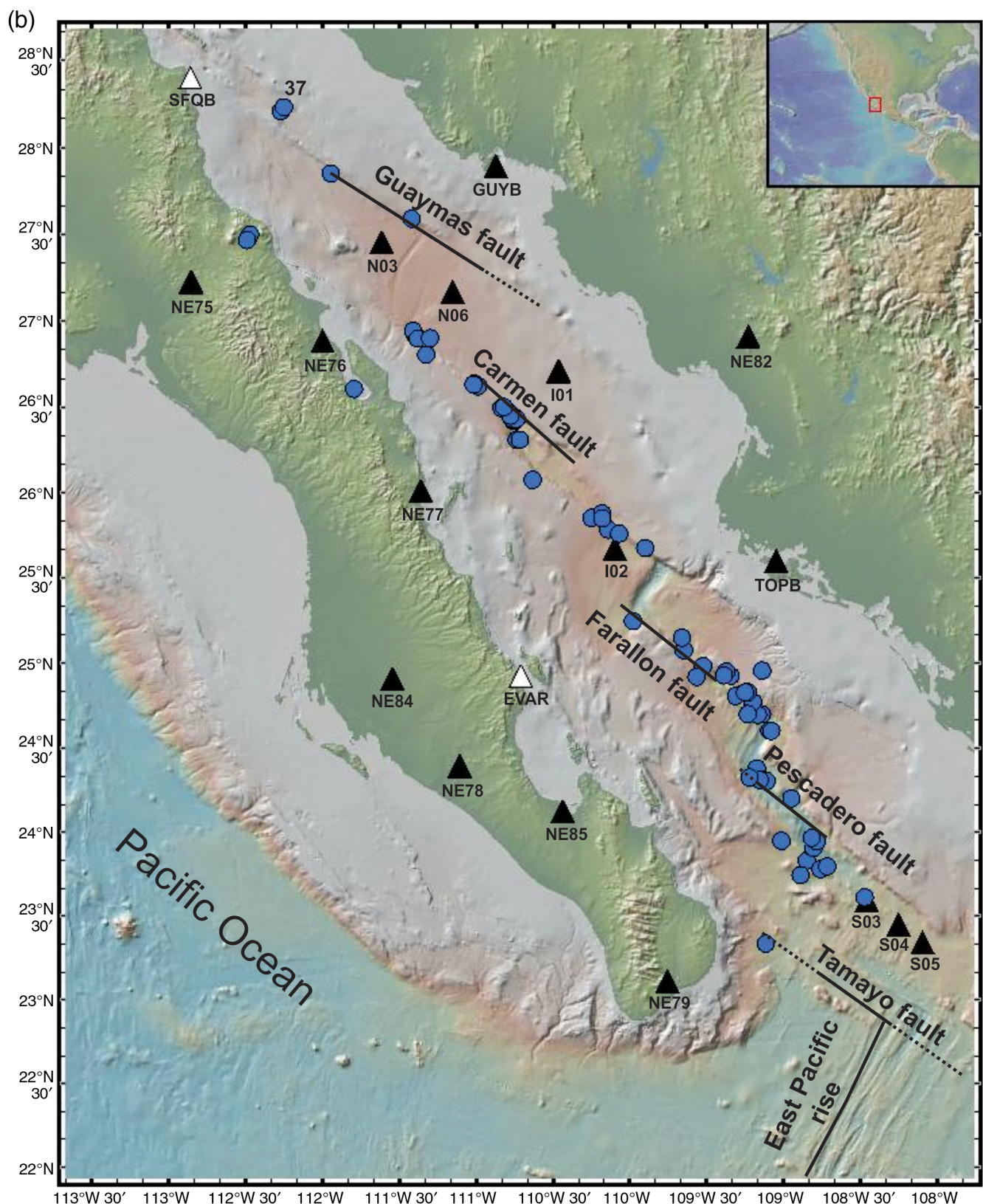


Figure 1. Continued.

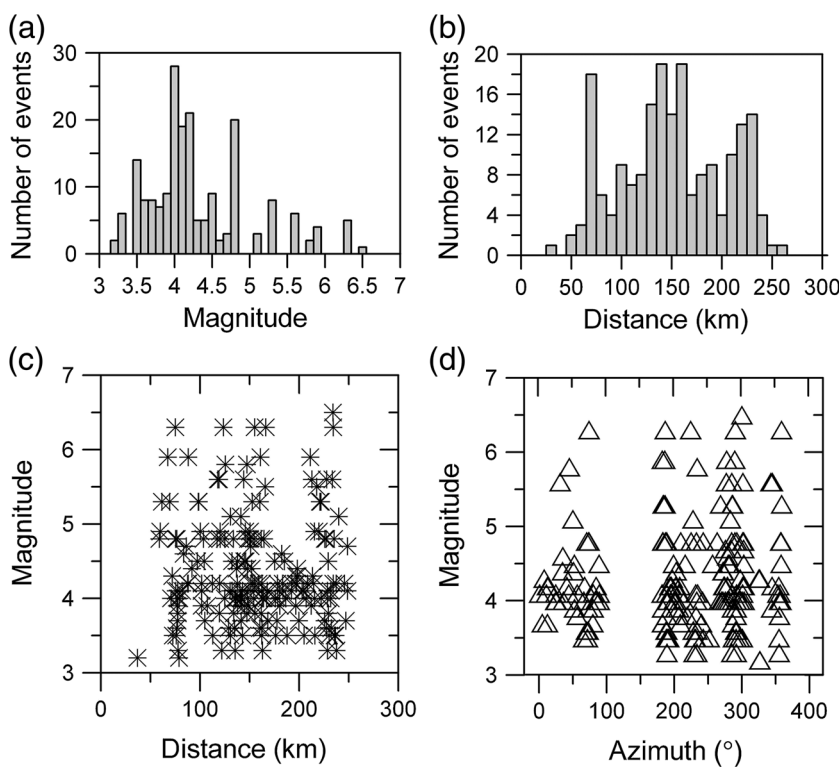


Figure 2. (a,b) Distribution of magnitude and epicentral distance in kilometers of the events analyzed. The frames at (c,d) show the distribution of (c) epicentral distance and (d) azimuth versus magnitude of the seismograms used.

set. They found that the attenuation of S waves is generally high ($Q_S \sim 50\text{--}180$). Castro *et al.* (2017a) determined Q_S using regional seismograms from earthquakes in the Farallon transform fault region, east of Loreto, Baja California Sur, in the south-central region of the GoC and found that $Q_S = 135f^{0.6}$. In a previous study, Castro and Avila-Barrientos (2015) determined the near-surface attenuation of the stations of the RESBAN array and found that most sites have an average near-surface attenuation parameter $K_0 \sim 0.03$ s.

Data

We analyzed 68 shallow earthquakes with focal depth of less than 23 km and magnitudes in the range of $3.2 \leq M \leq 6.5$ that were located by Sumy *et al.* (2013) and Castro *et al.* (2017a) in the southern GoC. The hypocenters determined by Sumy *et al.* (2013) come from events recorded from October 2005 to October 2006 by combining seismograms from an array of OBSs, of the SCOOBA experiment, with onshore stations of the NARS-Baja array. The earthquakes relocated by Castro *et al.* (2017b) in the same region occurred in the period April 2002 to December 2014 and were recorded by regional stations of the RESBAN operated by CICESE. Figure 1 shows the spatial distribution of the epicenters (circles) and the recording stations (black triangles) used in

this study. Because all the hypocenters used are located in the central and southern GoC, we only used stations located in this region. The map in Figure 1 also shows, as a reference, the location of other stations of the RESBAN array (white triangles) located farther north of the region of interest and the location of the main ridges and transform faults of the south-central GoC (Fig. 1b). The OBSs displayed in Figure 1 recorded all three components of motion with a rate of 32.25 samples per second. The stations of the NARS-Baja array recorded three-component ground velocity at the rate of 20 samples per second. We selected records having epicentral distances less than 250 km and having a signal-to-noise ratio above two. Figure 2 shows the distribution of the epicentral distances (Fig. 2c) and azimuths (Fig. 2d) with respect to the magnitude of the earthquakes analyzed. Most of the seismograms analyzed are in the distance range between 75 and 250 km and the magnitudes between 3.1 and 6.5. The source-station distance is uniformly distributed in that distance range and also provides nearly uniform azimuthal coverage. Because we did not analyze records south beyond the

GoC, there is an azimuthal gap between 100° and 190° (Fig. 2d). This gap, however, does not affect the region of interest sampled by the source-station rays.

The seismograms were baseline-corrected, and we selected time windows with clear S waves in the horizontal components to calculate acceleration spectral amplitudes. The lengths of the windows vary between 4 and 20 s depending on the source-station distance, starting with the first S -wave arrival and ending before the surface-wave arrivals. We tapered the beginning and the end of the time windows with a 5% cosine taper, and then calculated the Fourier transform and corrected the spectral amplitudes for instrument response. We smoothed the spectral records calculating the average amplitude of a variable frequency band of $\pm 25\%$ over 19 central frequencies, equidistant on a logarithmic scale between 0.25 and 7.94 Hz and selected amplitudes above noise level as in previous studies (Vidales-Basurto *et al.*, 2014; Avila-Barrientos and Castro, 2016). Figure 3a shows the acceleration spectra calculated from two horizontal-component seismograms recorded at different distances from an $M 4.8$ earthquake (event 37 labeled on lower frame of Fig. 1) located at the northwestern end of the Guaymas transform fault ($28.2360^\circ \text{N}, 112.2500^\circ \text{W}$). Figure 3b shows the acceleration spectra of the noise recorded before the P -wave arrival using the same window length selected for the S wave. The spectral amplitude of the noise is more than a factor of 2 below the spectral amplitudes of the signals.

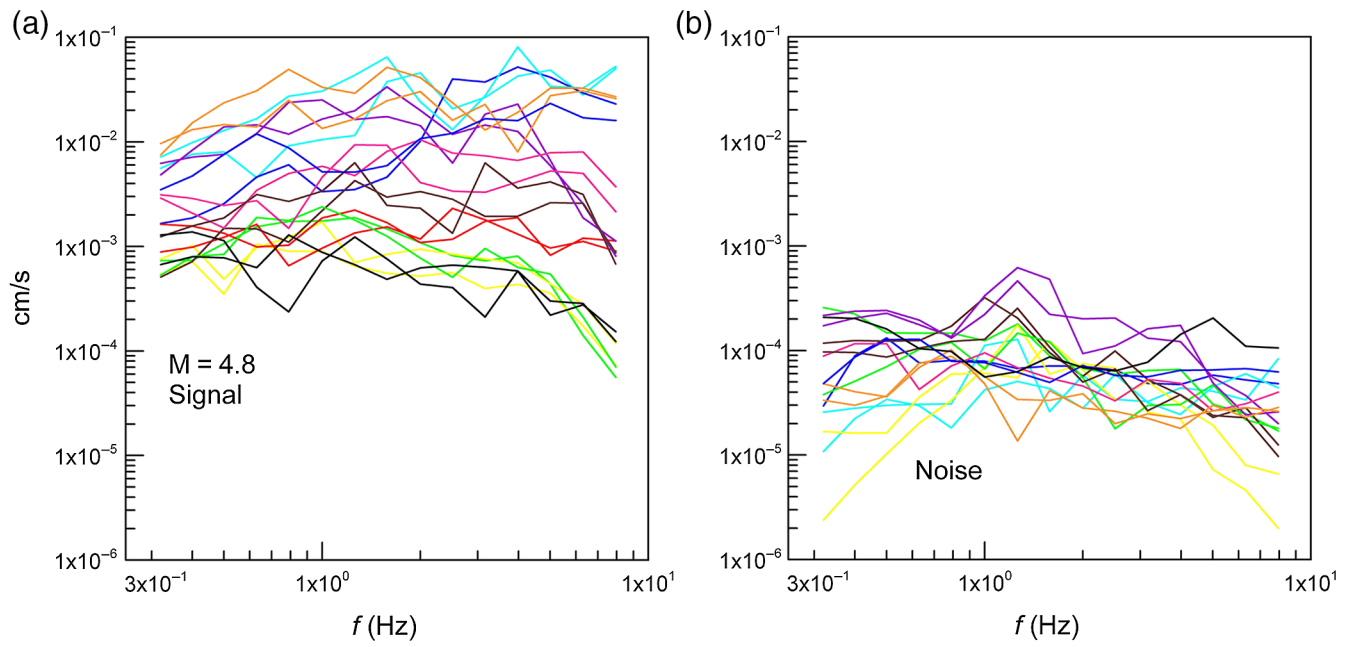


Figure 3. (a) Sample acceleration spectra from an earthquake with magnitude M_w 4.8 (event 37, labeled in lower frame of Fig. 1) recorded at stations located at different epicentral distances. We plotted both horizontal components (north-south and east-west). (b) The spectral amplitude of the seismic noise at each recording site. The color version of this figure is available only in the electronic edition.

Method

We first determined nonparametric attenuation functions that characterize the decay of the observed spectral amplitudes for a fixed frequency following the same method as Castro *et al.* (1990, 1996). These functions are obtained assuming that at a given frequency f , the observed spectral amplitudes $U_i(f, r)$ equal the product of a scalar $S_i(f)$ that depends on the earthquake size and accounts for source effects, and a nonparametric attenuation function $A(f, r)$ (hereafter, NAF) that describes how the spectral amplitudes decay with hypocentral distance r :

$$U_{ij}(f, r_j) = S_i(f)A(f, r_j). \quad (1)$$

In this nonparametric model, path-related effects such as site amplification are related to the residuals between the data points and the spectral amplitudes calculated with equation (1) and are separated from the NAF by a smoothing constraint (e.g., Castro *et al.*, 1990, 1996). The site response Z_k can be estimated as (Castro *et al.*, 2008)

$$Z_k = \frac{1}{N} \sum_{i=1}^N (U_{ij}^{\text{obs}} - U_{ij}^{\text{est}})_j \quad j = 1, \dots, L, \quad (2)$$

in which L is the number of distances sampled, N is the number of events recorded at site Z_k , and U_{ij}^{obs} is the observed and U_{ij}^{est} the estimated amplitudes using equation (1).

Vidales-Basurto *et al.* (2014) calculated NAF using site-corrected amplitudes and compared them with attenuation functions obtained with uncorrected spectral amplitudes

and they found small differences, particularly at short distances ($r < 100$ km).

We search for unrestricted monotonic curves for each frequency. This technique has been used before by Brillinger and Priesler (1984), Anderson and Quaas (1988), and Anderson (1991) to investigate the effect of magnitude on the decay of peak acceleration with distance. Malagnini and Herrmann (2000) and Malagnini *et al.* (2000) also used this method to estimate Q in the Apennines, Italy, and by Parolai *et al.* (2000, 2004), Bindi *et al.* (2004), and Oth *et al.* (2008, 2009) to study source and path effects.

We determine individual attenuation functions for each frequency and minimize possible site amplifications constraining $A(f, r)$ to slowly decrease with distance by adding a smoothness constraint. We also fix $A(f, 0) = 1.0$ because at $r = 0$ there is no attenuation. We linearize equation (1) by taking logarithms and for each frequency we solve a system of equations of the form:

$$u_{ij} = s_i + a_j, \quad (3)$$

in which $u_{ij} = \log U_{ij}(f, r_j)$ is a datum from earthquake i at distance j , $s_i = \log S_i(f)$, and $a_j = \log A(f, r_j)$ is the value of the attenuation function at distance j . The NAF includes implicitly the effect of scattering, intrinsic Q_S , and geometrical spreading, and provides a regional average of the attenuation parameters. Figure 4 displays a sample of NAF determined for frequencies between 0.5 and 8.0 Hz. The different rate of decay with distances shows that the attenuation depends on frequency.

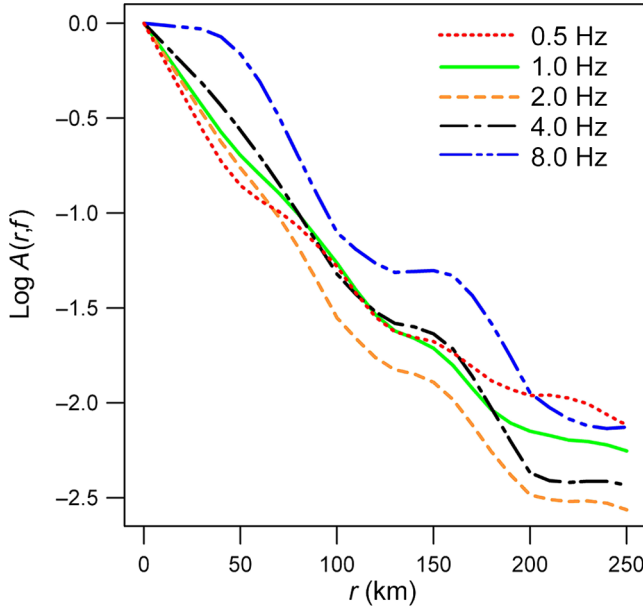


Figure 4. Nonparametric attenuation functions obtained for the five frequencies analyzed (0.5, 1.0, 2.0, 4.0, and 8.0 Hz). The color version of this figure is available only in the electronic edition.

Parametric Attenuation

We used the NAF to correct the observed spectral amplitudes for attenuation effects. Thus, the resulting functions $D_{ik}(f)$ contain only the product of source and site effects $Z_k(f)$:

$$D_{ik}(f) = \frac{U_{ij}(f, r_j)}{A(f, r_j)} = S_i(f)Z_k(f). \quad (4)$$

The ratio between the original observed spectral amplitudes and the function $D_{ik}(f)$ eliminates the source and site effects from the data and provides a specific link between source–station attenuation. Thus

$$\frac{U_{ij}(f, r_j)}{D_{ik}(f)} = A_{ij}(f, r_j). \quad (5)$$

The resulting attenuation functions can be parameterized as

$$A_{ij}(f, r_j) = G_{ij}(r_j) \exp\left[\frac{-\pi f r_{ij}}{Q_S \beta}\right], \quad (6)$$

in which $G_{ij}(r_j)$ represents the value of the geometrical spreading function between source i and station j , Q_S is the quality factor, and β is the velocity of the S waves. For a half-space, equation (6) can be written as

$$\log[A_{ij}(f, r_j)] - \log G_{ij}(r_j) = \frac{-\pi f r_{ij}}{\beta Q_S}. \quad (7)$$

We initially approximated the geometrical spreading as

$$G(r) = \begin{cases} 10/r & 10 < r < 100 \\ 10/\sqrt{100r} & r \geq 100 \end{cases}. \quad (8)$$

This function normalizes the amplitudes at 10 km and assumes dominance of body waves up to 100 km and decays at lower rate ($1/\sqrt{r}$) for distances greater than 100 km, where surface waves or refracted and reflected waves may have an effect on the spectral records. We choose a 10 km normalization factor because the NAFs (equations 1 and 3) were sampled every 10 km. The bilinear form of $G(r)$ is based on the geometrical spreading expected in a half-space, where seismic waves decay with distance proportionally to $1/r$ at short distances (e.g., $r < 100$ km) and to $1/\sqrt{r}$ for longer epicentral distances. A similar equation has been used before in other attenuation studies (Herrmann and Kijko, 1983; Castro *et al.*, 1990; Ordaz and Singh, 1992; among others). Thus, the use of equation (8) as a reference to estimates Q_S permits the comparison with other studies.

For a given frequency f and a layered space, equation (7) can be rewritten as

$$V_{ij} = C \sum_{k=1}^N \frac{r_{ijk}}{\beta_k Q_{S_k}}, \quad (9)$$

in which V_{ij} is the observed spectral amplitude from event i at site j corrected by source and site effects and also corrected by geometrical spreading using equation (8). The sub-index k refers to the layer. N is the number of layers and $C = \pi f$.

We use the 1D velocity model of González-Fernández *et al.* (2005), obtained from a 280-km-long seismic profile in the GoC, to calculate r_{ijk} by raytrace. Thus, the only unknown parameters in equation (9) are $1/Q_{S_k}$, which are obtained by a standard inversion procedure.

Results and Discussion

We determined average nonparametric attenuation functions (Fig. 4) that characterize the decay of the spectral amplitudes with distance and that show frequency dependence of the attenuation. The NAFs show an abrupt change in the amplitude decay between 100 and 150 km that could be related to the crust–upper-mantle transition. At this distance range, refracted and reflected waves from the Moho increase the spectral amplitudes decreasing the rate of amplitude decay with distance. Between 150 and 200 km, the rate of amplitude decay increases again when the Moho discontinuity affects less the spectral amplitudes. These functions also flatten between 200 and 250 km, a distance range where the seismic rays travel below the Moho through the more homogenous rocks of the upper mantle, where we would expect less scattering and more efficient S -wave propagation. Because the NAFs represent the average attenuation of the volume sampled with the source–station paths, we used them to eliminate the attenuation effect from the records

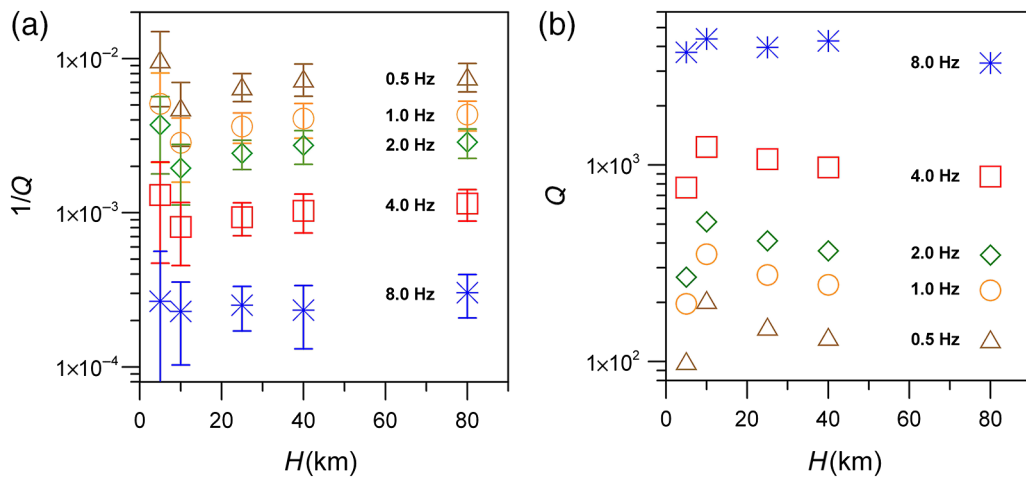


Figure 5. (a) Estimates of $1/Q \pm 1$ standard deviation versus depth (H) for the different frequencies analyzed (0.5, 1.0, 2.0, 4.0, and 8.0 Hz). Triangles are for 0.5 Hz, circles for 1 Hz, diamonds for 2 Hz, squares for 4 Hz, and asterisks for 8 Hz. (b) The corresponding values of Q of S waves calculated using the geometrical spreading function defined in equation (8). The color version of this figure is available only in the electronic edition.

(equation 4) and to find a specific source–station parametric function that permits the estimates of Q_S at different depths (equation 9).

Figure 5a shows the values of $1/Q_S$ obtained for a sample of five frequencies (0.5, 1, 2, 4, and 8 Hz) by inverting equation (9) using equation (8) to correct the spectral amplitudes for the geometrical spreading effect. Listing of the values of Q_S shown in Figure 5 is in Table 1. The values of Q_S (Fig. 5b) increase with frequency as found in previous studies in the GoC (Vidales-Basurto *et al.*, 2014; Castro *et al.*, 2017a). For all the frequencies analyzed, Q_S has low values at shallow depths ($H < 10$ km), increasing up to 10 km and slightly decreasing from 10 to 40 km depth. At 4 Hz, for instance, $Q_S \sim 770$ for the first 5 km, increasing to ~ 1200 up to 10 km depth where Q_S starts to gradually decrease, reaching a value of $Q_S \sim 970$ between 25 and 40 km depth. The increase of Q_S with depth may have important implications for ground-motion prediction. The estimates of Q_S at different depths permit us to evaluate how much seismic energy is attenuated near the source and how much along the source–station path. For instance, inslab earthquakes in central Mexico tend to have high values of pseudoacceleration response spectra at high frequencies, and they seem to increase with focal depth (Garcia *et al.*, 2005). A possible interpretation of this observation is that ray paths from deep events cross zones of high Q_S (Garcia *et al.*, 2005).

As mentioned before, previous studies in the GoC have found that $Q_S = 135f^{0.6}$ (Castro *et al.*, 2017a). For regional distances ($r > 100$ km) with source–station paths traveling mostly below the Moho, our model estimates values of Q_S at low frequencies ($f < 2$ Hz) that are consistent with that study. For instance, at 1 Hz and depths below 40 km, $Q_S \sim 200$. Flanagan and Wiens (1990) studied the attenuation characteristics beneath the Lau Spreading Center (central Tonga arc) and found low Q_S that tend to increase with focal depth, particularly below 200–300 km. They also found

low values of Q_S (~ 20 –35) near the spreading centers. Yang *et al.* (2007) used Rayleigh waves to estimate the intrinsic shear-wave quality factor near the East Pacific Rise, and they found values of Q in the 150–250 range between 10 and 30 km depth and in the 100–150 range between 30 and 50 km depth. This increase of attenuation at 30–50 km depth is consistent with the decrease of Q that we observe in the GoC at 10–40 km although our estimates of average Q are in general higher because the ray paths include spreading centers and the basins. These differences on the estimates of Q indicate that zones of high attenuation may be restricted to regions near the spreading centers where temperature is higher and the presence of melted rocks is likely. Eilon and Abers (2017), for instance, observed high attenuation ($Q_S < 25$) in a narrow zone of less than 50 km from the Juan de Fuca and Gorda ridge axes.

We also calculated Q_S using in equation (7) the geometrical spreading function $G(r) = 10/r$ for the whole distance range ($r \leq 250$ km). We compare in Figure 6 the estimates of Q_S obtained using equation (8) (triangles) and using $G(r) = 10/r$ (asterisks) for the geometrical spreading correction in equation (7). The trend of Q_S with depth is similar in both cases but lower values of Q_S are obtained when using equation (8) for the geometrical spreading, although within the error estimates.

To compare our estimates of Q_S with other studies, we calculate for each frequency the average Q_S weighting according with the thickness of the layers of the model. Figure 7 shows the weighted average Q_S versus frequency and the regression fit that gives the relation $Q_S = 223f^{1.2}$ (solid line). The squares (Fig. 7b) correspond to $Q_S = 176f^{0.6}$ obtained by Vidales-Basurto *et al.* (2014) using a smaller data set, with most events located between latitudes 26° – 28° N, and a geometrical spreading function similar to equation (8). The asterisks represent $Q_S = 135f^{0.6}$ obtained by Castro *et al.* (2017a) using events

Table 1
Listing of the Values of Q_S Shown in Figure 5

Depth (km)	$1/Q$ (0.5 Hz)	$\text{Err}1/Q$ (0.5 Hz)	Q (0.5 Hz)	$1/Q$ (1.0 Hz)	$\text{Err}1/Q$ (1.0 Hz)	Q (1.0 Hz)	$1/Q$ (2.0 Hz)	$\text{Err}1/Q$ (2.0 Hz)	Q (2.0 Hz)	$1/Q$ (4.0 Hz)	$\text{Err}1/Q$ (4.0 Hz)	Q (4.0 Hz)	$1/Q$ (8.0 Hz)	$\text{Err}1/Q$ (8.0 Hz)	Q (8.0 Hz)
5.0	0.1172	0.0453	8.53	0.0587	0.0220	17.02	0.0305	0.0115	32.73	0.0148	0.0056	67.64	0.0070	0.0026	142.35
10.0	0.0451	0.0186	22.17	0.0230	0.0094	43.53	0.0120	0.0049	83.23	0.0059	0.0024	170.33	0.0028	0.0011	361.27
25.0	0.0613	0.0118	16.30	0.0310	0.0060	32.27	0.0161	0.0031	62.07	0.0078	0.0015	128.05	0.0037	0.0007	270.40
40.0	0.0741	0.0152	13.49	0.0374	0.0077	26.73	0.0194	0.0040	51.55	0.0094	0.0019	106.38	0.0044	0.0009	225.91
80.0	0.0687	0.0139	14.55	0.0349	0.0070	28.69	0.0181	0.0037	55.20	0.0088	0.0018	113.68	0.0041	0.0008	242.35

The first column indicates the depth of the layer where Q was estimated. The rest of the columns list the estimates of $1/Q$, the standard error of the estimate, and the value of Q for 0.5, 1.0, 2.0, 4.0, and 8.0 Hz, respectively.

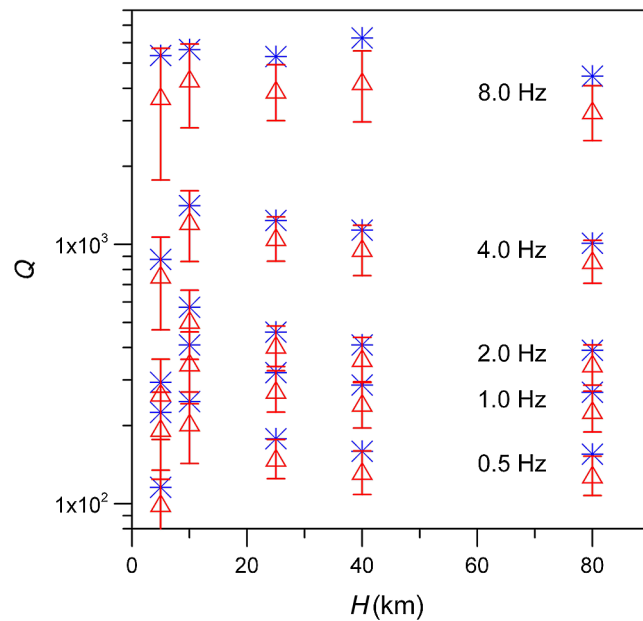


Figure 6. Estimates of Q versus depth (H) for the different frequencies analyzed (0.5, 1.0, 2.0, 4.0, and 8.0 Hz) using $G(r) = 10/r$ (asterisks) in equation (7) and using equation (8) (triangles) for the geometrical spreading correction. The color version of this figure is available only in the electronic edition.

located in the Farallon transform fault region (25° – 26° N) and $G(r) = \frac{10}{r^{0.9}}$ for the geometrical spreading. Along the Imperial fault, in the northern region of the GoC, [Singh et al. \(1982\)](#) found that $Q_S = 20f$ ($3 < f < 25$ Hz) below 4 km. Similarly, [Ho-Liu et al. \(1988\)](#) estimated that $Q_S \sim 20$ in the Brawley seismic zone at the 8–12 km depth. These results indicate that the quality factor of S waves in the GoC varies laterally considerably in space and in frequency as a result of the complex geologic structure. Q_S in other active regions, with a different tectonic regime, is lower than in the GoC. For instance, [Gupta and Kumar \(2002\)](#) found that $Q_S = 86f^{1.02}$ (diamonds in Fig. 7b) in northeast Himalaya and [Joshi \(2006\)](#) estimated that $Q_S = 112f^{0.97}$ in the central region of the Himalayan frontal arc (crosses in Fig. 7b). On the other extreme, Q tends to have high values in stable regions, such as in northern Spain where $Q_S = 600f^{0.45}$ ([Pujades et al., 1991](#); circles in Fig. 7b).

Conclusions

We obtained a 1D model for S waves that shows that Q_S increases with frequency ($0.5 \text{ Hz} \leq f \leq 8 \text{ Hz}$), but for a given frequency Q_S shows small variation with depth between 5 and 40 km, indicating that the Q_S -vertical structure of the crust in the south region of the GoC is approximately homogeneous. The geometrical spreading in the south region of the GoC can be approximated as $G(r) \sim 1/r$, which corresponds to the dominance of body waves at all distances. The values of Q_S estimated at low frequencies ($f < 4 \text{ Hz}$) using $G(r) = 10/r$ for the geometrical spreading function are similar to those estimated using a

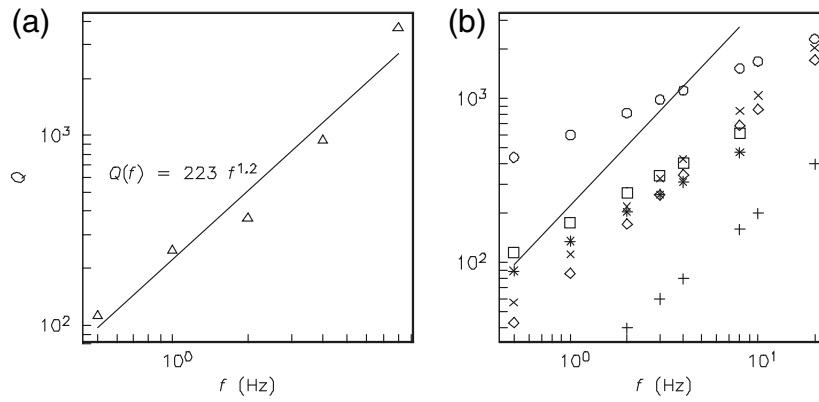


Figure 7. (a) The average values of Q_S (triangles) calculated for each frequency from the estimates of Q_S shown in Figure 5. The continuous straight line is the least-squares fit of the average values of Q_S obtained in this study. (b) The relation $Q_S = 223f^{1.2}$ obtained in this study is compared with estimates of Q_S by Vidales-Basurto *et al.* (2014; squares); $Q_S(f) = 135f^{0.6}$ (asterisks), obtained by Castro *et al.* (2017a); Q_S in the Imperial Valley (pluses; Singh *et al.* 1982); Q_S in northeast Himalaya (diamonds; Gupta and Kumar, 2002); Q_S in central Himalaya (crosses; Joshi, 2006); and Q_S in northern Spain (circles; Pujades *et al.*, 1991).

geometrical function that introduces a weaker decay with distance at $r > 100$ km (equation 8). At 4 Hz (the median frequency), $Q_S \sim 770\text{--}1200$ for the first 10 km, decreasing to $\sim 1070\text{--}970$ from 10 to 25 km depth. These values of Q_S sample a bigger volume and are higher than those obtained in previous studies. However, the decreasing Q_S at 10–25 km indicates that the amplitudes of S waves with deep source–station paths must attenuate more than those with shallow paths, in consistency with previous results obtained by Vidales-Basurto *et al.* (2014). The average values of Q_S determined in this study include attenuation near spreading centers, transform fault zones, basins, and short continental paths near the margins of the GoC. Therefore, comparing these average values of Q_S with those obtained near ridges in other attenuation studies (e.g., Eilon and Abers, 2017), we can conclude that the elastic characteristics in the GoC region must have important local lateral variations.

Data and Resources

Seismograms from the Network of Autonomously Recording Seismographs (NARS)-Baja array are available from the Incorporated Research Institutions for Seismology Data Management Center (IRIS-DMC) at <http://ds.iris.edu/mba/RB>. Some plots were made using Generic Mapping Tools (<http://www.soest.hawaii.edu/gmt>; Wessel and Smith, 1998). Some maps were made with GeoMapApp (<http://www.geomapapp.org>). All websites were last accessed on July 2018.

Acknowledgments

This Project was funded by Consejo Nacional de Ciencia y Tecnología (CONACYT) project Fondo para la Cooperación Internacional en Ciencia y Tecnología (FONCICYT)-CONACYT 1000/780/2016. The authors thank the technical support provided by Antonio Mendoza Camberos and

Arturo Pérez Vertti. The authors also thank the two anonymous reviewers and Associate Editor Thomas M. Brocher for their constructive comments and suggestions. Special thanks to Editor-in-Chief Thomas Pratt for considering the original article for the BSSA.

References

- Anderson, J. G. (1991). A preliminary descriptive model for the distance dependence of the spectral decay parameter in southern California, *Bull. Seismol. Soc. Am.* **81**, 2186–2193.
- Anderson, J. G., and R. Quaas (1988). The Mexico earthquake of September 19, 1985: Effect of magnitude on the character of strong ground motion: An example from Guerrero, Mexico strong motion network, *Earthq. Spectra* **4**, 635–646.
- Avila-Barrientos, L., and R. R. Castro (2016). Site response of the broad band stations of the NARS-Baja and RESBAN arrays, located in the region of the Gulf of California, México, *Geofis. Int.* **55**, 131–154.
- Axen, G. J., and M. J. Fletcher (1998). Late Miocene–Pleistocene extensional faulting, northern Gulf of California, Mexico and Salton trough, California, *Int. Geol. Rev.* **40**, 217–244.
- Bindi, D., R. R. Castro, G. Franceschina, L. Luzi, and F. Pacor (2004). The 1997–1998 Umbria-Marche sequence (central Italy): Source, path, and site effects estimated from strong motion data recorded in the epicentral area, *J. Geophys. Res.* **109**, no. B04312, doi: [10.1029/2003JB002857](https://doi.org/10.1029/2003JB002857).
- Brillinger, D. R., and H. K. Preisler (1984). An exploratory analysis of the Joyner–Boore attenuation data, *Bull. Seismol. Soc. Am.* **74**, 1441–1450.
- Castro, R. R., and L. Avila-Barrientos (2015). Estimation of the spectral parameter kappa in the region of the Gulf of California, Mexico, *J. Seismol.* **19**, 809–829.
- Castro, R. R., J. G. Anderson, and S. K. Singh (1990). Site response, attenuation and source spectra of S waves along the Guerrero, México, subduction zone, *Bull. Seismol. Soc. Am.* **80**, 1481–1503.
- Castro, R. R., M. R. Gallipoli, and M. Mucciarelli (2008). Crustal Q in southern Italy determined from regional earthquakes, *Tectonophysics* **457**, 96–101.
- Castro, R. R., F. Pacor, A. Sala, and C. Petrungaro (1996). S wave attenuation and site effects in the region of Friuli, Italy, *J. Geophys. Res.* **101**, 22,355–22,369.
- Castro, R. R., J. M. Stock, E. Hauksson, and R. Clayton (2017a). Source functions and path effects from earthquakes in the Farallon transform fault region, Gulf of California, Mexico that occurred on October 2013, *Pure Appl. Geophys.* **174**, no. 6, 2239–2256, doi: [10.1007/s00024-016-1346-4](https://doi.org/10.1007/s00024-016-1346-4).
- Castro, R. R., J. M. Stock, E. Hauksson, and R. Clayton (2017b). Active tectonics in the Gulf of California and seismicity ($M > 3.0$) for the period 2002–2014, *Tectonophysics* **719/720**, 4–16, doi: [10.1016/j.tecto.2017.02.015](https://doi.org/10.1016/j.tecto.2017.02.015).
- Eberhart-Phillips, D., M. Chadwick, and S. Bannister (2008). Three-dimensional attenuation structure of central and southern South Island, New Zealand, from local earthquakes, *J. Geophys. Res.* **113**, no. B05308, doi: [10.1029/2007JB005369](https://doi.org/10.1029/2007JB005369).
- Eberhart-Phillips, D., G. McVerry, and M. Reyners (2010). Influence of the 3D distribution of Q and crustal structure on ground motions from the 2003 M_w 7.2 Fiordland, New Zealand, earthquake, *Bull. Seismol. Soc. Am.* **100**, 1225–1240.
- Eilon, Z. C., and G. A. Abers (2017). High seismic attenuation at a mid-ocean ridge reveals the distribution of deep melt, *Sci. Adv.* **3**, no. 5, e1602829.

- Flanagan, M. P., and D. A. Wiens (1990). Attenuation structure beneath the Lau back arc spreading center from teleseismic S phases, *Geophys. Res. Lett.* **17**, 2117–2120.
- Garcia, D., S. K. Singh, M. Herraiz, M. Ordaz, and J. F. Pacheco (2005). Inslab earthquakes of central Mexico: Peak ground-motion parameters and response spectra, *Bull. Seismol. Soc. Am.* **95**, 2272–2282.
- González-Fernández, A., J. J. Dañobeitia, L. A. Delgado-Argote, F. Michaud, D. Cordoba, and R. Bartolomé (2005). Mode of extension and rifting history of upper Tiburón and upper Delfín basins, northern Gulf of California, *J. Geophys. Res.* **110**, no. B01313, doi: [10.1029/2003JB002941](https://doi.org/10.1029/2003JB002941).
- Graizer, V., and E. Kalkan (2015). Update of the Graizer–Kalkan ground-motion prediction equations for shallow crustal continental earthquakes, *U.S. Geol. Surv. Open-File Rept. 2015-1009*, 79 pp., doi: [10.3133/ofr20151009](https://doi.org/10.3133/ofr20151009).
- Gupta, S. C., and A. Kumar (2002). Seismic wave attenuation characteristics of three Indian regions: A comparative study, *Curr. Sci.* **82**, 407–413.
- Herrmann, R. B., and A. Kijko (1983). Modeling some empirical vertical component *Lg* relations, *Bull. Seismol. Soc. Am.* **73**, 157–171.
- Ho-Liu, P., H. Kanamori, and R. W. Clayton (1988). Applications of attenuation tomography to Imperial Valley and Coso–Indian wells region, southern California, *J. Geophys. Res.* **93**, no. B9, 10,501–10,520.
- Joshi, A. (2006). Use of acceleration spectra for determining the frequency-dependent attenuation coefficient and source parameters, *Bull. Seismol. Soc. Am.* **96**, 2165–2180.
- Lizarralde, D., G. J. Axen, H. E. Brown, J. M. Fletcher, A. Gonzalez-Fernandez, A. J. Harding, W. S. Holbrook, G. M. Kent, P. Paramo, and F. Sutherland (2007). Variation in styles of rifting in the Gulf of California, *Nature* **448**, 466–469.
- Lonsdale, P. F. (1989). Geology and tectonic history of the Gulf of California, in *The Eastern Pacific Ocean and Hawaii*, E. L. Winterer, D. M. Hussong, and R. W. Decker (Editors), Geol. Soc. Am., Denver, Colorado, 499–521.
- Malagnini, L., and R. B. Herrmann (2000). Ground-motion scaling in the region of the 1997 Umbria–Marche earthquake (Italy), *Bull. Seismol. Soc. Am.* **90**, 1041–1051.
- Malagnini, L., R. B. Herrmann, and M. Di Bona (2000). Ground-motion scaling in the Apennines (Italy), *Bull. Seismol. Soc. Am.* **90**, 1062–1081.
- Ordaz, M., and S. K. Singh (1992). Source spectra and spectral attenuation of seismic waves from Mexican earthquakes, and evidence of amplification in the hill zone of Mexico City, *Bull. Seismol. Soc. Am.* **82**, 24–43.
- Oskin, M., J. Stock, and A. Martin-Barajas (2001). Rapid localization of Pacific–North America plate motion in the Gulf of California, *Geology* **29**, 459–462.
- Oth, A., D. Bindi, S. Parolai, and F. Wenze (2008). S-wave attenuation characteristics beneath the Vrancea region in Romania: New insights from the inversion of ground-motion spectra, *Bull. Seismol. Soc. Am.* **98**, 2482–2497.
- Oth, A., D. Bindi, S. Parolai, and F. Wenze (2009). Source spectra and site response from S waves of intermediate-depth Vrancea, Romania, earthquakes, *Bull. Seismol. Soc. Am.* **99**, 235–254.
- Parolai, S., D. Bindi, and P. Augliera (2000). Application of the generalized inversion technique (GIT) to a microzonation study: Numerical simulations and comparison with different site-estimation techniques, *Bull. Seismol. Soc. Am.* **90**, 286–297.
- Parolai, S., D. Bindi, M. Baumbach, H. Grosser, C. Milkereit, S. Karalisa, and S. Zünbül (2004). Comparison of different site response estimation techniques using aftershocks of the 1999 Izmit earthquake, *Bull. Seismol. Soc. Am.* **94**, 1096–1108.
- Pujades, L., J. A. Canas, J. J. Egocue, M. A. Puigví, J. Pous, J. Gallart, X. Lana, and A. Casas (1991). Coda Q distribution in Iberian Peninsula, *Geophys. J. Int.* **100**, 285–301.
- Singh, S. K., R. J. Apsel, J. Fried, and J. N. Brune (1982). Spectral attenuation of SH waves along the Imperial fault, *Bull. Seismol. Soc. Am.* **72**, 2003–2016.
- Stock, J. M., and K. V. Hodges (1989). Pre-Pliocene extension around the Gulf of California and the transfer of Baja California to the Pacific plate, *Tectonics* **8**, 99–115.
- Sumy, D. F., J. B. Gaherty, W.-Y. Kim, T. Diehl, and J. A. Collins (2013). The mechanism of earthquakes and faulting in the southern Gulf of California, *Bull. Seismol. Soc. Am.* **103**, 487–506.
- Thatcher, W., and J. Brune (1971). Seismic study of an oceanic ridge earthquake swarm in the Gulf of California, *Geophys. J. Roy. Astron. Soc.* **22**, 473–489.
- Vidales-Basurto, C. A., R. R. Castro, C. I. Huerta, D. F. Sumy, J. B. Gaherty, and J. A. Collins (2014). An attenuation study of body-waves in the south-central region of the Gulf of California, México, *Bull. Seismol. Soc. Am.* **104**, 2027–2042, doi: [10.1785/0120140015](https://doi.org/10.1785/0120140015).
- Wessel, P., and W. H. F. Smith (1998). New, improved version of generic mapping tools released, *Eos Trans. AGU* **79**, no. 47, 579.
- Yang, Y., D. W. Forsyth, and D. S. Weeraratne (2007). Seismic attenuation near the East Pacific Rise and the origin of the low-velocity zone, *Earth Planet. Sci. Lett.* **258**, 260–268.

Departamento de Sismología
División Ciencias de la Tierra
Centro de Investigación Científica y de Educación Superior de Ensenada (CICESE)
Carretera Tijuana-Ensenada No. 3918
22860 Ensenada, Baja California
Mexico
raul@cicese.mx
(R.R.C.)

Instituto de Geofísica, UNAM
Ciudad Universitaria
04510 México, D.F.
Mexico
(S.K.S.)

Department of Earth Sciences
Indian Institute of Technology, Roorkee
Roorkee 247667, Uttarakhand
India
(A.J., S.S.)

Manuscript received 22 August 2018;
Published Online 19 February 2019